



EUCENTRE
FOR YOUR SAFETY.

ERIES-RESTORING Test Report

REtrofitting of STOne masonRy using INnovative Grid-based composites

User Group:

Madalena Ponte ^{1,2}, Larisa Garcia- Ramonda ³,
Francesco Graziotti ², Anastasios Tsiavos ⁴, Luca Pelà ³, Andrea
Penna ², Guido Magenes ², Rita Bento ¹, Gabriele Guerrini ²

Research Infrastructure staff:

Igor Lanese ⁵, Elisa Rizzo Parisi ⁵, Filippo Dacarro ⁵, Maria Pia
Scovenna ⁵, Gerard J. O'Reilly ⁶

¹ CERIS, Instituto Superior Técnico, Universidade de Lisboa

² Department of Civil Engineering and Architecture, University of
Pavia

³ Department of Civil and Environmental Engineering, Universitat
Politécnica de Catalunya (UPC-BarcelonaTech)

⁴ Department of Civil, Environmental and Geomatic Engineering, ETH
Zurich

⁵ European Centre for Training and Research in Earthquake
Engineering (EUCENTRE)

⁶ University School for Advanced Studies (IUSS)

Order protocol

2022.EUC.003

ERIES-RESTORING Test Report

REtrofitting of STOne masonRy using INnovative Grid-based composites

Report ID: ERIES-RESTORING_Test_Report

Document	Written pages:	Total pages:
Test Report	40	47

Issue:	Revision:	Revision:	Revision:
November 28 th , 2024	-	-	-

File Name:	Order protocol
ERIES-RESTORING_Test_Report.pdf	2022.EUC.003

According to law, the EUCENTRE Foundation trademark cannot be reproduced, copied or utilized, without the written permission of the EUCENTRE Foundation, which is the owner. This report has been released on the basis of the results obtained during the experimental tests carried out by the EUCENTRE Foundation. Any release, partial reproduction or modification of any element contained herein, without the written authorization of the EUCENTRE Foundation, is strictly prohibited. This report may be reproduced only in its entirety and for the purposes authorized by law. The EUCENTRE Foundation refuses any responsibility for the incorrect use of data contained therein, or for the use of any total, partial or modified copies without obtaining prior authorization.

According to law, the EUCENTRE Foundation trademark cannot be reproduced, copied, or utilized, without the written permission of the EUCENTRE Foundation, which is the owner. This report has been released on the basis of the results obtained during the experimental tests carried out by the EUCENTRE Foundation. Any release, partial reproduction, or modification of any element contained herein, without the written authorization of the EUCENTRE Foundation, is strictly prohibited. This report may be reproduced only in its entirety and for the purposes authorized by law. The EUCENTRE Foundation refuses any responsibility for the incorrect use of data contained therein, or for the use of any total, partial, or modified copies without obtaining prior authorization.

Description

This Test Report provides a description of the experimental campaign of the ERIES-RESTORING project, carried out at the EUCENTRE-IUSS Research infrastructure within the framework of ERIES (www.eries.eu).

The ERIES project (Engineering Research Infrastructures for European Synergies) is funded by the European Commission's Horizon Europe program. Coordinated by the Scuola Universitaria Superiore IUSS Pavia in Italy, it has a budget of €11.6 million and has a four-year duration, from 2022 to 2026.

ERIES aims to provide transnational access to advanced research infrastructures in structural, seismic, wind, and geotechnical engineering. The project seeks to enhance resilience against natural hazards such as earthquakes and extreme winds by fostering innovative and sustainable solutions to mitigate economic losses and social disruptions. Additionally, it develops new technical standards and methodologies to improve built environment safety and supports frontier research through international collaboration.

The ERIES network includes 13 partners from 8 countries across Europe and North America, such as the University of Bristol, the Laboratório Nacional de Engenharia Civil (Portugal), and Western University (Canada).

This Test Report describes the specimens' geometry, material properties, test set-up and protocol, instrumentation layout, and dataset organization.

Table of Contents

1	Introduction.....	9
2	Characterization of constituent materials.....	11
2.1	Stone properties.....	11
2.2	Mortar properties.....	11
2.3	GFRP mesh properties.....	11
2.4	Helicoidal connector properties.....	11
3	Specimens description.....	13
3.1	Vertical compression test specimens.....	14
3.2	Diagonal compression test specimens.....	16
3.3	Quasi-static cyclic shear-compression test specimens.....	17
3.4	Overview of specimen designation.....	20
4	Vertical compression tests.....	21
4.1	Set-up.....	21
4.2	Testing protocol.....	21
4.3	Instrumentation.....	21
4.4	Data acquisition, processing, and distribution.....	23
5	Diagonal compression tests.....	25
5.1	Set-up.....	25
5.2	Testing protocol.....	25
5.3	Instrumentation.....	25
5.4	Data acquisition, processing, and distribution.....	26
6	Quasi-static cyclic shear-compression tests on piers.....	29
6.1	Set-up.....	29
6.2	Testing protocol.....	33
6.3	Instrumentation.....	37
6.4	Data acquisition, processing, and distribution.....	40
	Acknowledgments.....	45
	References.....	47

Index of Tables

Table 1.	Mechanical properties of the masonry and retrofit mortars.....	12
Table 2.	Vertical compression test specimens' designation.....	14
Table 3.	Diagonal compression test specimens' designation.....	16
Table 4.	Test specimen combinations and designation.....	19
Table 5.	Overview of the specimens tested.....	20
Table 6.	Actual gauge lengths of potentiometers in vertical compression tests. Units of mm.....	22
Table 7.	Data matrix description for vertical compression tests.....	23
Table 8.	Actual gauge lengths of potentiometers in diagonal compression tests. Units of mm.....	26
Table 9.	Data matrix description for diagonal compression tests.....	27
Table 10.	Lateral loading protocol for the slender pier specimens, where three repetitions of each loading cycle were applied at every target drift ratio.....	35
Table 11.	Lateral loading protocol for the squat pier specimens, where three repetitions of each loading cycle were applied at every target drift ratio.....	36
Table 12.	Data matrix description for quasi-static cyclic shear-compression tests on slender piers.....	41
Table 13.	Data matrix description for quasi-static cyclic shear-compression tests on squat piers.....	42

Index of Figures

Figure 1. Mechanical characterization tests on mortar prisms: (a) three-point bending tests; (b) vertical compression tests.....	12
Figure 2. Construction of the double-leaf stone masonry walls.....	13
Figure 3. Detail of the helicoidal connectors: (a) CRM retrofit; (b) FRM retrofit	14
Figure 4. Finished look of the masonry long walls while curing and while being cut into wallettes to be tested under vertical compression.....	15
Figure 5. Dimensions of the wallettes for vertical compression tests. Units of cm.	15
Figure 6. Jacketing system mesh and connector placement on a specimen for vertical compression tests.	15
Figure 7. Finished look of the long masonry wall while curing and being cut into wallettes to be tested under diagonal compression.....	16
Figure 8. Dimensions of the wallettes for diagonal compression tests. Units of cm.	16
Figure 9. Jacketing system mesh and connector placement on a specimen for diagonal compression tests.	17
Figure 10. Quasi-static cyclic shear-compression test specimen dimensions: (a) slender piers with aspect ratio $h/l = 1.5$, and (b) squat piers with aspect ratio $h/l = 0.69$. Units of cm.....	18
Figure 11. Jacketing system mesh and connector placement: (a) CRM on slender piers, (b) CRM on squat piers, and (c) FRM on slender pier.	19
Figure 12. Vertical compression test set-up.	21
Figure 13. Instrumentation layout of the vertical compression test specimens.	22
Figure 14. Diagonal compression test set-up.	25
Figure 15. Instrumentation layout of the diagonal compression test specimens.	26
Figure 16. Quasi-static cyclic shear-compression test set-up: (a) slender and (b) squat specimens.	29
Figure 17. Quasi-static cyclic shear-compression test set-up for pier SQ_URM: (a) side view, and (b) front view. Units of cm.....	30
Figure 18. Quasi-static cyclic shear-compression test set-up for piers SL_URM, SL_CRM1, and SL_CRM2: (a) side view, and (b) front view. Units of cm.	31
Figure 19. Quasi-static cyclic shear-compression test set-up for piers SQ_CRM1 and SQ_CRM2: (a) side view, and (b) front view. Units of cm.....	32
Figure 20. Quasi-static cyclic shear-compression test set-up for pier SL_FRM2: (a) side view, and (b) front view. Units of cm.....	33
Figure 21. Scheme of the vertical forces applied to the RC beam.....	34
Figure 22. Instrumentation on the back and side façades: (a) squat, and (b) slender piers.	37
Figure 23. Instrumentation layout for the squat pier specimens.	38
Figure 24. Instrumentation layout for the slender pier specimens.	39
Figure 25. Random speckle pattern for the DIC method.	40

1 Introduction

In recent decades, there has been an increasing interest in the development of retrofitting solutions for ancient unreinforced masonry buildings, as past seismic events have highlighted the high vulnerability of these structures. The correct choice of compatible materials that ensure the intervention's efficiency, sustainability, and durability plays a critical role; thus, techniques based on polymeric meshes embedded in inorganic matrices, preferably lime-based mortars, have gained increasing appeal for the retrofit of historic unreinforced masonry buildings. Among these solutions, we find Fabric Reinforced Cementitious Matrices (FRCM) and Composite Reinforced Mortars (CRM). In addition, other solutions that do not require the installation of textiles or grids, like Fiber-Reinforced Mortars (FRM), have also been recently introduced in the retrofitting of masonry buildings. However, all of these techniques are still not fully codified as structural retrofits, and experimental results on their effectiveness are needed to develop the necessary design guidelines.

The work presented in this report is part of the ERIES project, which provides transnational access to leading experimental facilities. This experimental program, named ERIES-RESTORING, was a multiteam work led by the University of Lisbon (Portugal) in collaboration with the University of Pavia (Italy), Universitat Politècnica de Catalunya (Spain), EUCENTRE Foundation, and IUSS Pavia (Italy), and initial contributions from ETH Zurich (Switzerland). A quasi-static cyclic shear-compression testing campaign was conducted at the EUCENTRE Foundation laboratories in Pavia, Italy, while mechanical characterization tests, including vertical and diagonal compression tests on masonry, were carried out at the Material and Structural Testing Laboratory of the Department of Civil Engineering and Architecture (DICAr) of the University of Pavia. The ERIES-RESTORING project aims to bridge the information gap about the seismic effectiveness of Composite Reinforced Mortars (CRM) and Fibre Reinforced Mortars (FRM) when applied to existing undressed stone masonry walls. The specimens studied in the experimental campaign were built to represent the current conditions of ancient buildings typical of European and Mediterranean countries, usually constructed of double-leaf natural stone masonry with roughly dressed blocks obtained from sedimentary rocks.

To achieve this objective, the campaign included: (i) characterization tests on mortar samples from the stone masonry and the jacketing systems, (ii) nine vertical and nine diagonal compression tests on bare and retrofitted with CRM masonry wallettes, and (iii) seven cyclic shear-compression tests on bare and retrofitted full-scale masonry piers with two different aspect ratios. Mechanical properties of stones, reinforcing meshes, and helicoidal connectors were taken from technical sheets or other official testing certificates, provided by the supplier. The experimental campaign addressed four configurations of undressed stone masonry: unreinforced (bare) condition, serving as a reference; CRM strengthening on one side of the wall; CRM strengthening on both sides; and FRM strengthening on both sides. For the quasi-static cyclic shear-compression tests campaign, the retrofit configurations were studied for two height/length aspect ratios of 1.5 (slender piers) and 0.69 (squat piers).

This report provides a comprehensive account of the mechanical properties of the constituent materials of masonry and retrofit (Section 2), along with the geometric characteristics and construction details of the specimens (Section 3) built for three types of tests: vertical compression, diagonal compression, and quasi-static cyclic shear-compression tests. The essential information about the

experimental methods, such as testing protocols, instrumentation plans, and dataset organization, are presented in Sections 4, 5, and 6.

All test data are available with this report at the following DOI: [10.60756/euc-vbua48i530](https://doi.org/10.60756/euc-vbua48i530). The authors make this information available to help other researchers replicating the tests or developing analytical and numerical models to study the seismic behavior enhancement of retrofitted stone masonry buildings.

2 Characterization of constituent materials

2.1 Stone properties

Natural stones were cut from Credaro-Berrettino calcareous sandstone rocks in the province of Bergamo, Italy. According to the quarry documentation, they were characterized by a mean density of 2580 kg/m³, mean compressive strength of 149 MPa perpendicular and 144 MPa parallel to the sedimentation layers, and mean tensile strength of 19 MPa.

2.2 Mortar properties

The mortar mix design for the construction of the masonry walls required special attention in order to obtain a weak hydraulic-lime mortar comparable with the overall masonry properties typically encountered in historical buildings. To ensure compatibility between the substrate and the strengthening solution, the CRM retrofit mortar also contained a fraction of natural hydraulic lime. Instead, the mortar mix used for the FRM solution was based on a pozzolan hydraulic binder with polyvinyl-alcohol fibers. Both CRM and FRM retrofit mortars are made and distributed by Ruregold with the commercial names MX-CP Calce¹ and MX-PVA Fibrorinforzata², respectively. The tensile (f_{mt}) and compressive (f_{mc}) strength of the masonry and strengthening mortars were obtained through standard laboratory tests (Figure 1a and b) and are shown in Table 1. According to the procedure established by EN 1015-11 (CEN, 2006), the mortar was cast in prisms with dimensions of 160 x 40 x 40 mm and was tested after 28 days of curing.

2.3 GFRP mesh properties

The GFRP meshes embedded in the CRM strengthening of the specimens, with the commercial name G-MESH 400³, were characterized by mean tensile strengths of 74 kN/m and 86 kN/m in the weft and warp directions (f_{weft} and f_{warp}), respectively, and an ultimate strain ε_{fu} of 1.5% in both directions, according to the material characterization carried out by other research facilities for the supplier. The weft of the GFRP mesh is spaced 120 mm apart and the warp 80 mm apart, for a total fiber weight of 400 g/m².

2.4 Helicoidal connector properties

Based on the supplier's technical sheets, the helicoidal steel connectors, with the commercial name Connettore Elicoidale⁴, were made of stainless steel AISI 304 with a nominal diameter of 10 mm.

¹ <https://ruregold.com/it/wp-content/uploads/2023/05/Scheda-Tecnica-MX-CP-Calce.pdf>

² <https://ruregold.com/it/wp-content/uploads/2023/06/Scheda-Tecnica-MX-PVA-Fibrorinforzata.pdf>

³ <https://ruregold.com/it/wp-content/uploads/2023/05/Scheda-Tecnica-G-MESH-400-1.pdf>

⁴ <https://ruregold.com/wp-content/uploads/2023/05/scheda-tecnica-CONNETTORE-ELICOIDALE-ruregold.pdf>



Figure 1. Mechanical characterization tests on mortar prisms: (a) three-point bending tests; (b) vertical compression tests.

Table 1. Mechanical properties of the masonry and retrofit mortars.

	Masonry walls		CRM retrofit		FRM retrofit	
	f_{mc} [MPa]	f_{mt} [MPa]	f_{mc} [MPa]	f_{mt} [MPa]	f_{mc} [MPa]	f_{mt} [MPa]
Mean	0.81	0.17	22.55	5.84	47.02	6.91
C.o.V.	33%	72%	12%	9%	19%	7%

3 Specimens description

The specimens studied in the experimental campaign were built to represent the current conditions of ancient buildings typical of European and Mediterranean countries, usually constructed of double-leaf natural stone masonry with roughly dressed blocks obtained from sedimentary rocks. The stones were roughly shaped with a hammer, presenting dimensions between approximately 100 and 300 mm. The specimens' construction comprised two layers of stone arranged in uneven horizontal courses, separated by mortar layers about 5 to 20 mm thick. The space between the two leaves of stone varied according to the stones' irregularities and was filled with mortar and stone scraps (Figure 2). No through stones were provided except at the pier and wall edges. The final nominal thickness of the masonry was about 300 mm for all specimens.

The CRM retrofit consisted of a glass-FRP (GFRP) mesh embedded in a mortar with a nominal thickness of 30 mm; however, it should be considered that the masonry' irregular surface resulted in non-uniform thickness of the mortar jacket. The CRM and FRM layers were mechanically connected to the wall by helicoidal steel bars with an approximate density of five per square meter of façade, as shown in Figure 3. Helicoidal connectors passed through both masonry leaves and were bent into the retrofit mortar when the jackets were applied on both sides, while they were embedded into about $\frac{3}{4}$ of the specimen thickness (approximately 25 cm long) when the retrofit was applied to only one side. In both cases, they also provided transverse passive confinement to the masonry. Polymeric discs were provided with the connectors to help against stress concentration in the jackets.



Figure 2. Construction of the double-leaf stone masonry walls.

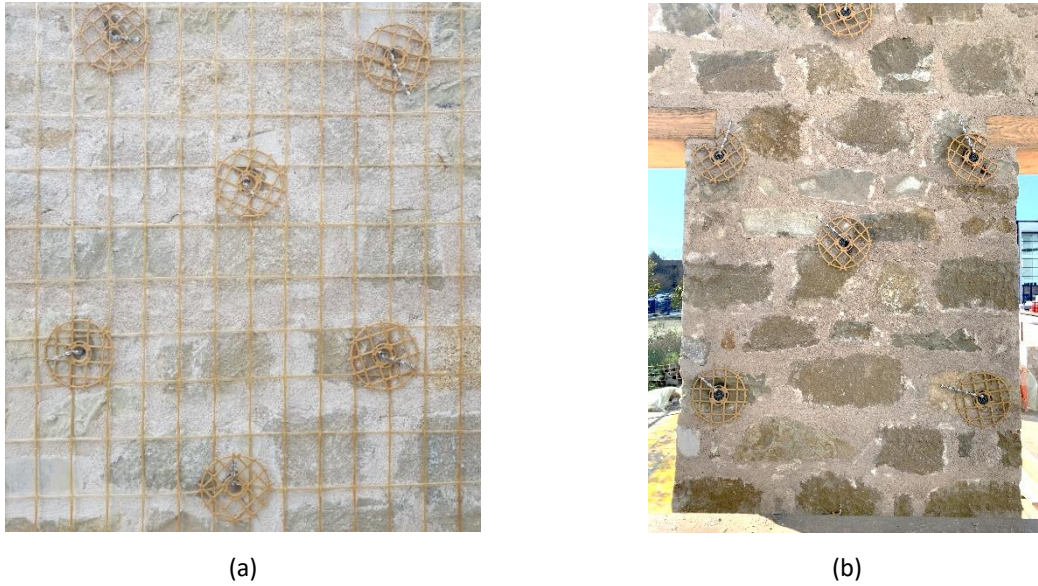


Figure 3. Detail of the helicoidal connectors: (a) CRM retrofit; (b) FRM retrofit

3.1 Vertical compression test specimens

Nine wallettes were tested under vertical compression in three different configurations: bare masonry, CRM on one side, and CRM on two sides. This campaign did not include vertical compression tests with the FRM retrofit. For each configuration, three wallettes were tested. The test specimens were named as in Table 2.

Table 2. Vertical compression test specimens' designation.

Configuration	Specimen designation
Unreinforced masonry	V_URM_1, V_URM_2, V_URM_3
Masonry with CRM on one side	V_CRM1_1, V_CRM1_2, V_CRM1_3
Masonry with CRM on both sides	V_CRM2_1, V_CRM2_2, V_CRM2_3

The wallettes were saw-cut from a long wall (Figure 4), discarding a 400 mm length at the extremities to avoid the confining effects of through stones necessary at the wall edges for construction (Magenes et al., 2010; Senaldi et al., 2018). Reinforced concrete (RC) spreader beams were provided at the top and bottom of the wall to distribute the load during testing and to facilitate transportation. The wall was first stabilized using vertical steel ties that applied a light pre-compression to minimize potential damage during cutting and transport. An electric circular saw with a water-cooled steel-diamond blade, mounted on a metallic guide affixed to the wall, was then used to cut the wallettes after 28 days of curing.



Figure 4. Finished look of the masonry long walls while curing and while being cut into wallettes to be tested under vertical compression.

The dimensions of the specimens were 120 x 80 x 30 cm (Figure 5), adapting the specifications of EN 1052-1 (CEN, 1998), to accommodate the average size of irregular stones instead of standard brick block dimensions, since standard dimensions are not available for stone masonry. After saw-cutting, the CRM was applied to the selected specimens (Figure 6). The GFRP mesh was mounted with the warp horizontal.

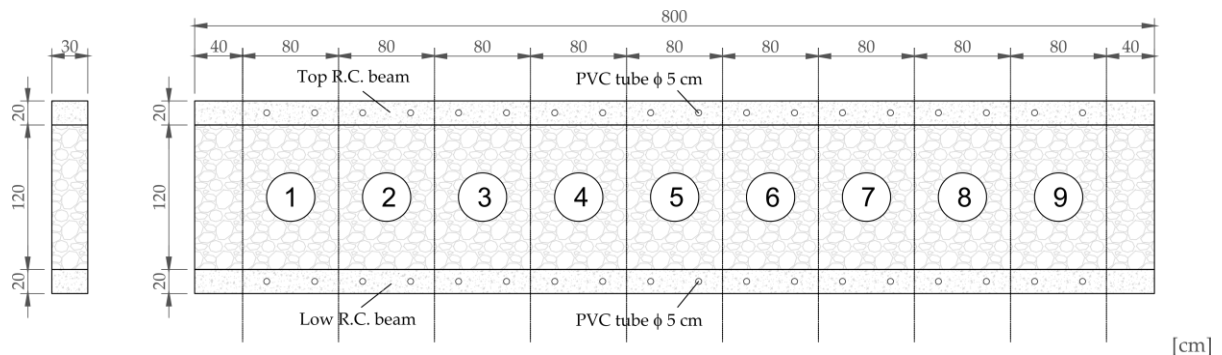


Figure 5. Dimensions of the wallettes for vertical compression tests. Units of cm.



Figure 6. Jacketing system mesh and connector placement on a specimen for vertical compression tests.

3.2 Diagonal compression test specimens

Nine wallettes were tested under diagonal compression in three different configurations: bare masonry, CRM on one side, and CRM on two sides. This campaign did not include diagonal compression tests with the FRM retrofit. For each configuration, three wallettes were tested. The test specimens were named as in Table 3.

Table 3. Diagonal compression test specimens' designation.

Configuration	Specimen designation
Unreinforced masonry	D_URM_1, D_URM_2, D_URM_3
Masonry with CRM on one side	D_CRM1_1, D_CRM1_2, D_CRM1_3
Masonry with CRM on both sides	D_CRM2_1, D_CRM2_2, D_CRM2_3

The wallettes were saw-cut from a long wall (Figure 7), discarding a 400 mm length at the extremities to avoid the confining effects of through stones necessary at the wall edges for construction (Magenes et al., 2010; Senaldi et al., 2018). Spreader beams were not provided to the wall because they would have interfered with the test set-up and execution. The wall was first stabilized using vertical steel ties that applied a light pre-compression to minimize potential damage during cutting and transport. An electric circular saw with a water-cooled steel-diamond blade, mounted on a metallic guide affixed to the wall, was then used to cut the wallettes after 28 days of curing.



Figure 7. Finished look of the long masonry wall while curing and being cut into wallettes to be tested under diagonal compression.

The dimensions of the specimens were 100 x 100 x 30 cm, following the specifications of ASTM (2015) and RILEM (1991), as presented in Figure 8. After saw-cutting, the CRM was applied to the selected specimens (Figure 9).

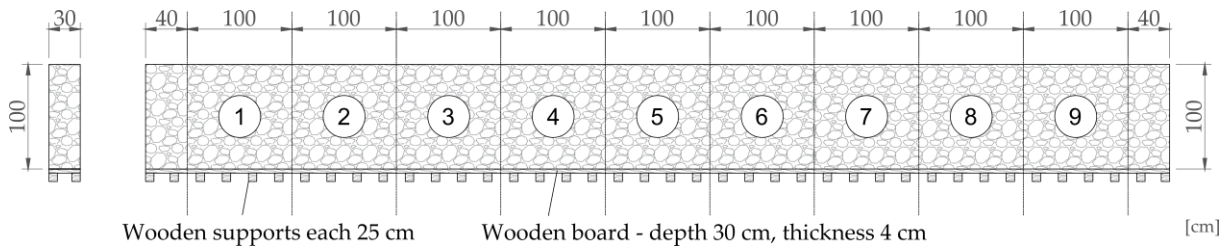


Figure 8. Dimensions of the wallettes for diagonal compression tests. Units of cm.



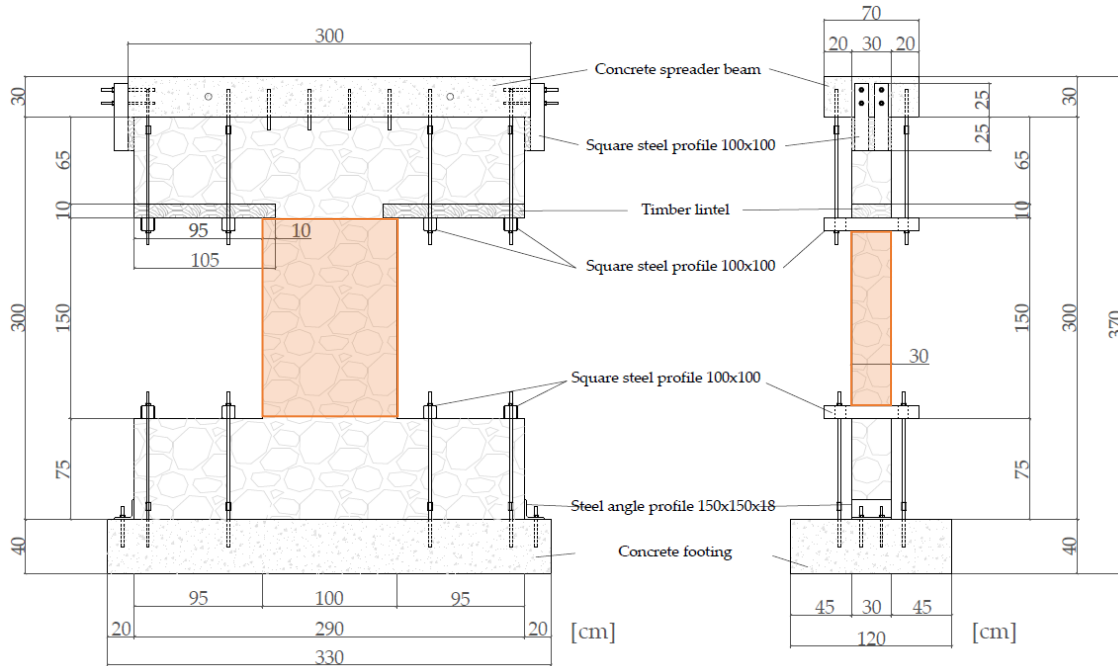
Figure 9. Jacketing system mesh and connector placement on a specimen for diagonal compression tests.

3.3 Quasi-static cyclic shear-compression test specimens

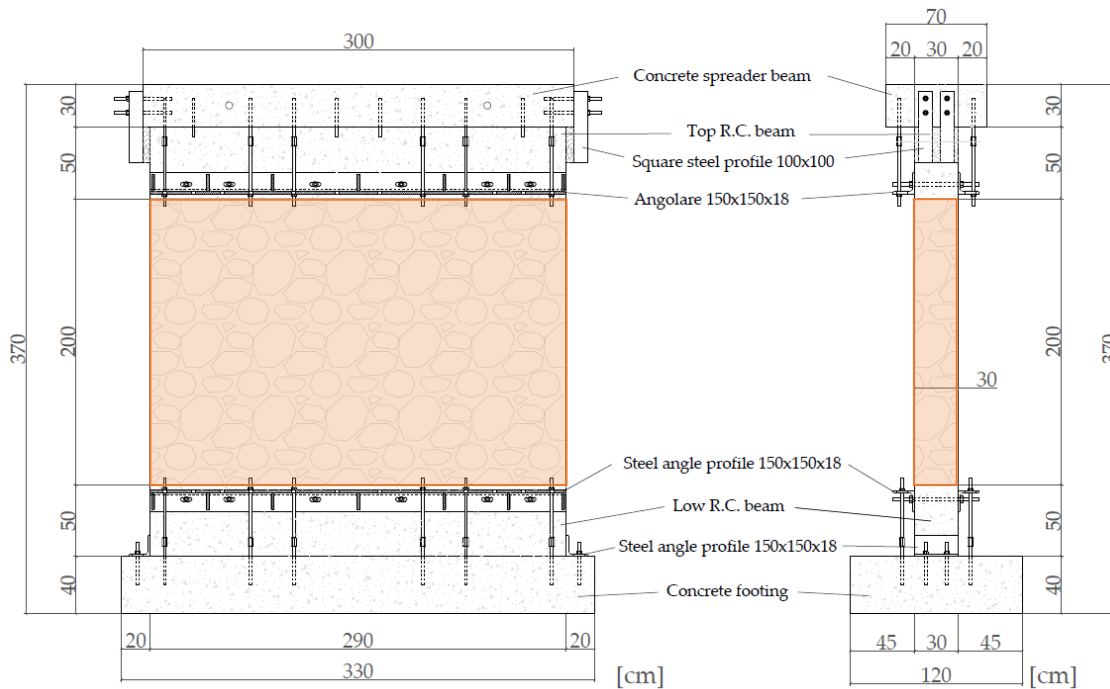
The quasi-static cyclic shear-compression tests were performed on seven pier specimens built with the same natural stone masonry previously described. No through stones were provided, except at the pier or spandrel vertical edges on alternated courses. Two different pier geometries were considered with height/length aspect ratios $h/l = 1.5$ (slender piers, Figure 10a) and $h/l = 0.69$ (squat piers, Figure 10b). The slender specimens included portions of the adjacent spandrels to allow CRM anchorage in the nodal panel, as in the case of masonry piers between windows. The squat piers corresponded to walls without openings or with large spacing between them and were completed by top and bottom RC beams where the GFRP mesh was anchored. Combining retrofit configurations and pier geometries resulted in seven specimens, as presented and named in Table 4.

A connection system made of threaded bars and steel profiles, shown in Figure 10, was designed to prevent rocking or sliding between each specimen and the RC foundation or spreader beam. The number of bars used for this connection system depended on the forces involved in each specimen. A set of 8 bars was used for the top and bottom connections of the slender piers (see Figure 18), except for the pier retrofitted with FRM, which required 12 bars top and bottom (see also Figure 20). For the squat piers, 16 bars were provided at the top and bottom in the URM configuration (see Figure 15), while 20 bars were used at the top and bottom in the strengthened ones (see Figure 19).

The meshes of the CRM retrofit were applied with the warp in the vertical direction for the squat piers and in the horizontal direction for the slender ones, to force the squat piers to fail in shear and the slender ones in flexure. Some connectors were applied to the RC beams of the squat specimens to provide flexural anchorage for the strengthening. Where necessary, the mesh was lap-spliced for at least 300 mm (Figure 11).



(a)



(b)

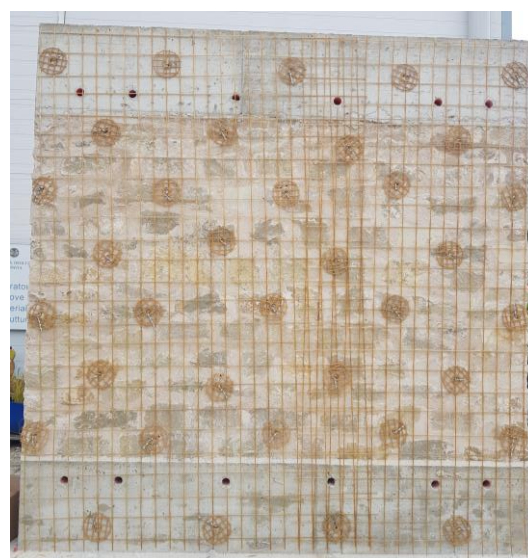
Figure 10. Quasi-static cyclic shear-compression test specimen dimensions: (a) slender piers with aspect ratio $h/l = 1.5$, and (b) squat piers with aspect ratio $h/l = 0.69$. Units of cm.

Table 4. Test specimen combinations and designation.

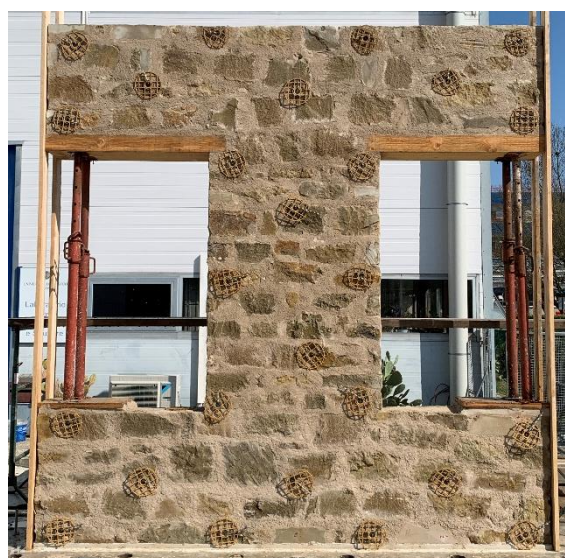
Configuration	Aspect ratio (h/l)	Specimen designation
Unreinforced masonry	0.69	SQ_URM
	1.5	SL_URM
Masonry with CRM on one side	0.69	SQ_CRM1
	1.5	SL_CRM1
Masonry with CRM on both sides	0.69	SQ_CRM2
	1.5	SL_CRM2
Masonry with FRM on both sides	1.5	SL_FRM2



(a)



(b)



(c)

Figure 11. Jacketing system mesh and connector placement: (a) CRM on slender piers, (b) CRM on squat piers, and (c) FRM on slender pier.

3.4 Overview of specimen designation

Table 5 provides an overview of the specimens tested within this project.

Table 5. Overview of the specimens tested.

Test type	Configuration	Specimen designation
Vertical compression	Unreinforced masonry	V_URM_1
		V_URM_2
		V_URM_3
	Masonry with CRM on one side	V_CRM1_1
		V_CRM1_2
		V_CRM1_3
	Masonry with CRM on both sides	V_CRM2_1
		V_CRM2_2
		V_CRM2_3
Diagonal compression	Unreinforced masonry	D_URM_1
		D_URM_2
		D_URM_3
	Masonry with CRM on one side	D_CRM1_1
		D_CRM1_2
		D_CRM1_3
	Masonry with CRM on both sides	D_CRM2_1
		D_CRM2_2
		D_CRM2_3
Quasi-static cyclic shear-compression	Unreinforced masonry	SQ_URM
		SL_URM
	Masonry with CRM on one side	SQ_CRM1
		SL_CRM1
	Masonry with CRM on both sides	SQ_CRM2
		SL_CRM2
	Masonry with FRM on both sides	SL_FRM2

4 Vertical compression tests

The wallettes were subjected to vertical compression tests by applying loading and unloading cycles of increasing amplitude to assess the mechanical properties of bare and retrofitted stone masonry, like the Young's modulus, Poisson's ratio, and vertical compressive strength. The following sections describe the experimental set-up, the testing protocol, the instrumentation plan, and the data acquisition, processing, and distribution.

4.1 Set-up

A force-controlled universal testing machine and displacement transducers constitute the testing apparatus, as shown in Figure 12. The applied axial compression was centered on the wallette and distributed as uniformly as possible on the cross-section by reinforced concrete spreader beams. In addition, the upper and lower faces of the beams, which were in contact with the machine, were regularized with a thin layer of gypsum.



Figure 12. Vertical compression test set-up.

4.2 Testing protocol

The testing protocol consisted of a vertical load applied at a controlled rate, ensuring a smooth, shock-free application. Loading and unloading cycles were characterized by amplitudes of $1/6$, $1/3$, and $1/2$ of the expected strength estimated from previous tests available in the literature on similar materials (Senaldi et al., 2018; Guerrini et al., 2021), with durations of the ramps of 210, 420, and 630 seconds, respectively. Then, the specimens were loaded monotonically to failure. Maximum and zero loads of each cycle were held constant for about 10 seconds before the unloading or reloading phase to stabilize the stress state.

4.3 Instrumentation

The deformations were measured by eight 50-mm-stroke potentiometers, located as shown in Figure 13. Vertical strains were measured using four displacement transducers (numbers 2, 3, 5, and 6 in Figure 13), while two transducers (numbers 4 and 7) were used to capture horizontal strains within the

wallette plane, and other two (numbers 8 and 9) were placed to measure horizontal strains across the wallette thickness. To ensure accurate measurements, the mounting rods of the transducers were installed in stones of sufficient size, avoiding mortar joints. Consequently, the nominal length between the mounting rods was adjusted case-by-case, and the actual gauge lengths are presented in Table 6. The instrumentation was installed within the middle half of the panel, where it is assumed that the influence of boundary effects on the stress state is sufficiently small.

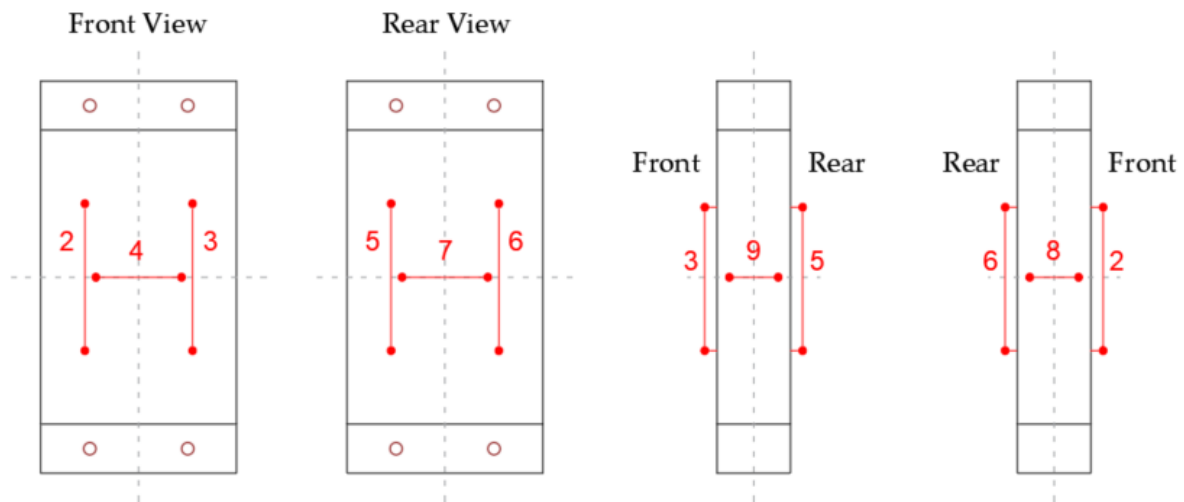


Figure 13. Instrumentation layout of the vertical compression test specimens.

Table 6. Actual gauge lengths of potentiometers in vertical compression tests. Units of mm.

Specimen designation	Sensor ID							
	2	3	4	5	6	7	8	9
V_URM_1	611	602	396	603	607	394	206	200
V_URM_2	612	605	406	618	607	407	211	196
V_URM_3	620	619	402	635	612	395	198	196
V_CRM1_1	614	610	400	622	605	404	200	196
V_CRM1_2	600	612	400	603	565	410	210	200
V_CRM1_3	616	610	395	620	613	409	200	206
V_CRM2_1	608	605	399	607	605	397	210	192
V_CRM2_2	620	614	408	610	611	400	206	204
V_CRM2_3	598	612	395	610	620	394	210	211

The values in light grey correspond to transducers recording unreliable data.

4.4 Data acquisition, processing, and distribution

All data sets are organized in .txt files shared online with DOI 10.60756/euc-vbua48i530 and named as the specimen designation in Table 2. Data are organized in columns corresponding to the time series recorded by each instrument, as presented in Table 7. In particular:

- i. Column 1 provides the time at a sampling rate of 5Hz;
- ii. Columns 2 through 9 provide the displacement time histories measured by the linear potentiometers;
- iii. Column 10 provides the forces applied by the machine.

Positive displacements correspond to elongation of the potentiometers. Positive forces are in tension. The force and displacement histories were zeroed at the beginning of each test using the average of the first ten values.

Table 7. Data matrix description for vertical compression tests.

Column No.	Sensor ID	Sensor type	Measured quantity / Instrument location	Units
1	-	-	Time	s
2	2	Linear potentiometer	Vertical disp., pier, front face, left side	mm
3	3	Linear potentiometer	Vertical disp., pier, front face, right side	mm
4	4	Linear potentiometer	Horizontal disp., pier, front face, mid-height	mm
5	5	Linear potentiometer	Vertical disp., pier, rear face, left side	mm
6	6	Linear potentiometer	Vertical disp., pier, rear face, right side	mm
7	7	Linear potentiometer	Horizontal disp., pier, rear face, mid-height	mm
8	8	Linear potentiometer	Horizontal disp., pier, side face, mid-height	mm
9	9	Linear potentiometer	Horizontal disp., pier, side face, mid-height	mm
10	F	Load cell	Machine vertical force, top, centered	kN

5 Diagonal compression tests

The wallettes were subjected to diagonal compression tests by applying loading and unloading cycles of increasing amplitude to assess the mechanical properties of bare and retrofitted stone masonry, like the shear stiffness and strength. The following sections describe the experimental set-up, testing protocol, the instrumentation plan, and the data acquisition, processing, and distribution.

5.1 Set-up

A force-controlled universal testing machine, the same as the one used for the vertical compression tests, and displacement transducers constitute the testing apparatus, as shown in Figure 14. The applied axial compression was centered on the diagonal of the wallette, leaving the other diagonal unloaded. In addition, the two corners of the wallette, which were in contact with the machine, were regularized with a thin layer of gypsum.



Figure 14. Diagonal compression test set-up.

5.2 Testing protocol

The testing protocol consisted of a vertical load applied at a controlled rate, ensuring a smooth, shock-free application. Loading and unloading cycles were characterized by load-controlled amplitudes of $1/6$, $1/3$, and $1/2$ of the expected strength estimated from previous tests available in the literature on similar materials (Senaldi et al., 2018; Guerrini et al., 2021), with durations of the ramps of 100, 200, and 300 seconds, respectively. Then, the specimens were loaded monotonically to failure. Maximum and zero loads of each cycle were held constant for about 10 seconds before the unloading or reloading phase to stabilize the stress state.

5.3 Instrumentation

The deformations were measured by four 50-mm-stroke potentiometers, located as shown in Figure 15. Vertical strains were measured using two displacement transducers (numbers 2 and 4 in Figure 15), while two transducers (numbers 3 and 5 in Figure 15) were used to capture horizontal strains within the wallette plane. To ensure accurate measurements, the mounting rods of the transducers

were installed in stones of sufficient size, avoiding mortar joints. Consequently, the nominal length between the mounting rods was adjusted case-by-case, and the actual gauge lengths are presented in Table 8. The instrumentation was installed within the middle half of the panel, where it is assumed that the influence of boundary effects on the stress state is sufficiently small.

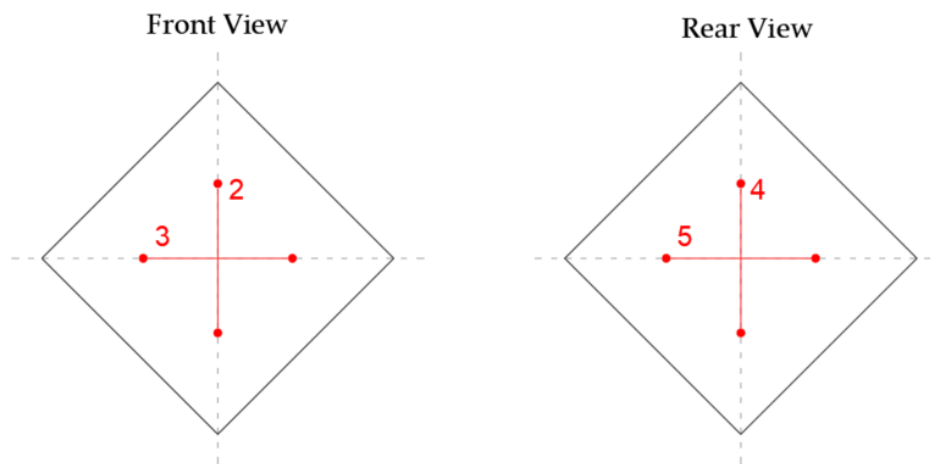


Figure 15. Instrumentation layout of the diagonal compression test specimens.

Table 8. Actual gauge lengths of potentiometers in diagonal compression tests. Units of mm.

Specimen designation	Sensor ID			
	2	3	4	5
D_URM_1	647	587	605	607
D_URM_2	608	607	604	651
D_URM_3	604	600	611	607
D_CRM1_1	605	615	513	565
D_CRM1_2	610	605	623	690
D_CRM1_3	1145	1141	1062	1100
D_CRM2_1	1142	1124	1122	1132
D_CRM2_2	615	605	621	606
D_CRM2_3	605	605	615	607

The values in light grey correspond to transducers recording unreliable data.

5.4 Data acquisition, processing, and distribution

All data sets are organized in .txt files shared online with DOI 10.60756/euc-vbua48i530 and named as the specimen designation in Table 3. Data are organized in columns corresponding to the time series recorded by each instrument, as presented in Table 7. In particular:

- Column 1 provides the time at a sampling rate of 5Hz;
- Columns 2 through 5 provide the displacement time histories measured by the linear potentiometers;
- Column 6 provides the forces applied by the machine.

Positive displacements correspond to elongation of the potentiometers. Positive forces are in tension. The force and displacement histories were zeroed at the beginning of each test using the average of the first ten values.

ERIES-RESTORING Test Report

Table 9. Data matrix description for diagonal compression tests.

Column No.	Sensor ID	Sensor type	Measured quantity / Instrument location	Units
1	-	-	Time	s
2	2	Linear potentiometer	Vertical disp., pier, front face	mm
3	3	Linear potentiometer	Horizontal disp., pier, front face	mm
4	4	Linear potentiometer	Vertical disp., pier, rear face	mm
5	5	Linear potentiometer	Horizontal disp., pier, rear face,	mm
6	F	Load cell	Machine vertical force, top, centered	kN

6 Quasi-static cyclic shear-compression tests on piers

The specimens were subjected to quasi-static cyclic shear-compression tests by applying push-and-pull lateral displacement cycles of increasing amplitude under constant axial load, to assess the damage evolution, failure modes, deformation capacity, and lateral strength of the bare and retrofitted stone masonry. The following sections describe the experimental test set-up, the testing protocol, the instrumentation plan, and the data acquisition, processing, and distribution.

6.1 Set-up

The experimental set-up for in-plane cyclic tests exploited the three-dimensional strong-wall/strong-floor configuration available at the EUCENTRE laboratory (Magenes et al., 2010), as shown in Figure 16. Three servo-hydraulic actuators were connected to a steel beam securely attached to the RC spreader beam: two vertical actuators were positioned on top of the specimens, symmetrically to the centreline of the masonry pier, and applied a constant axial load and boundary conditions by controlling the top rotation. The horizontal actuator induced the lateral displacements on the top RC spreader beam placed above each specimen to ensure the uniform distribution of the loads. The specimens were built on top of an RC foundation beam, which was fastened to the strong floor of the laboratory using post-tensioned steel threaded bars. Additionally, specific restraints were in place to prevent out-of-plane displacements of the pier top, allowing only longitudinal translation.

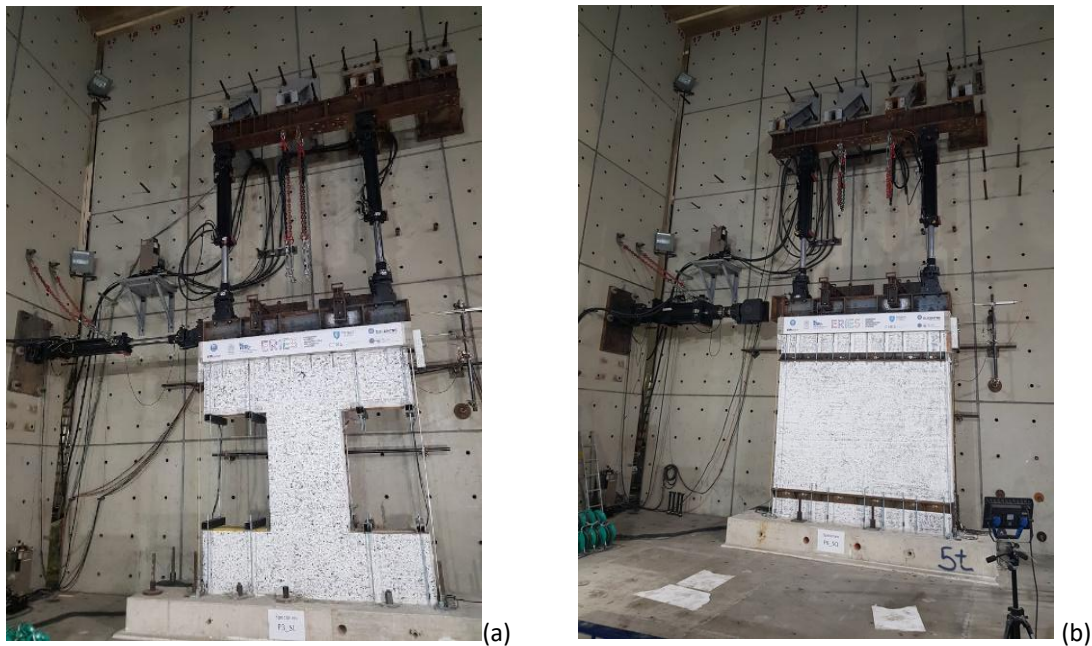


Figure 16. Quasi-static cyclic shear-compression test set-up: (a) slender and (b) squat specimens.

Two sets of actuators were employed to accommodate the large range of strength of the tested specimens. For the specimens with low expected resistance, i.e. the bare masonry squat pier (SQ_URM) and CRM-strengthened slender piers (SL_URM, SL_CRM1, and SL_CRM2), a horizontal actuator with a maximum force capacity of 500 kN in tension/compression and vertical actuators with a maximum force capacity of 250 kN in tension and 500 kN in compression were used (Figure 17 and Figure 18). Instead, for the two CRM-strengthened squat piers (SQ_CRM1 and SQ_CRM2) and the FRM-strengthened slender pier (CL_FRM2), a horizontal actuator with a maximum force capacity of 1000 kN in tension/compression and vertical actuators with a maximum force capacity of 500 kN in tension/compression were required, as shown in Figure 19 and Figure 20.

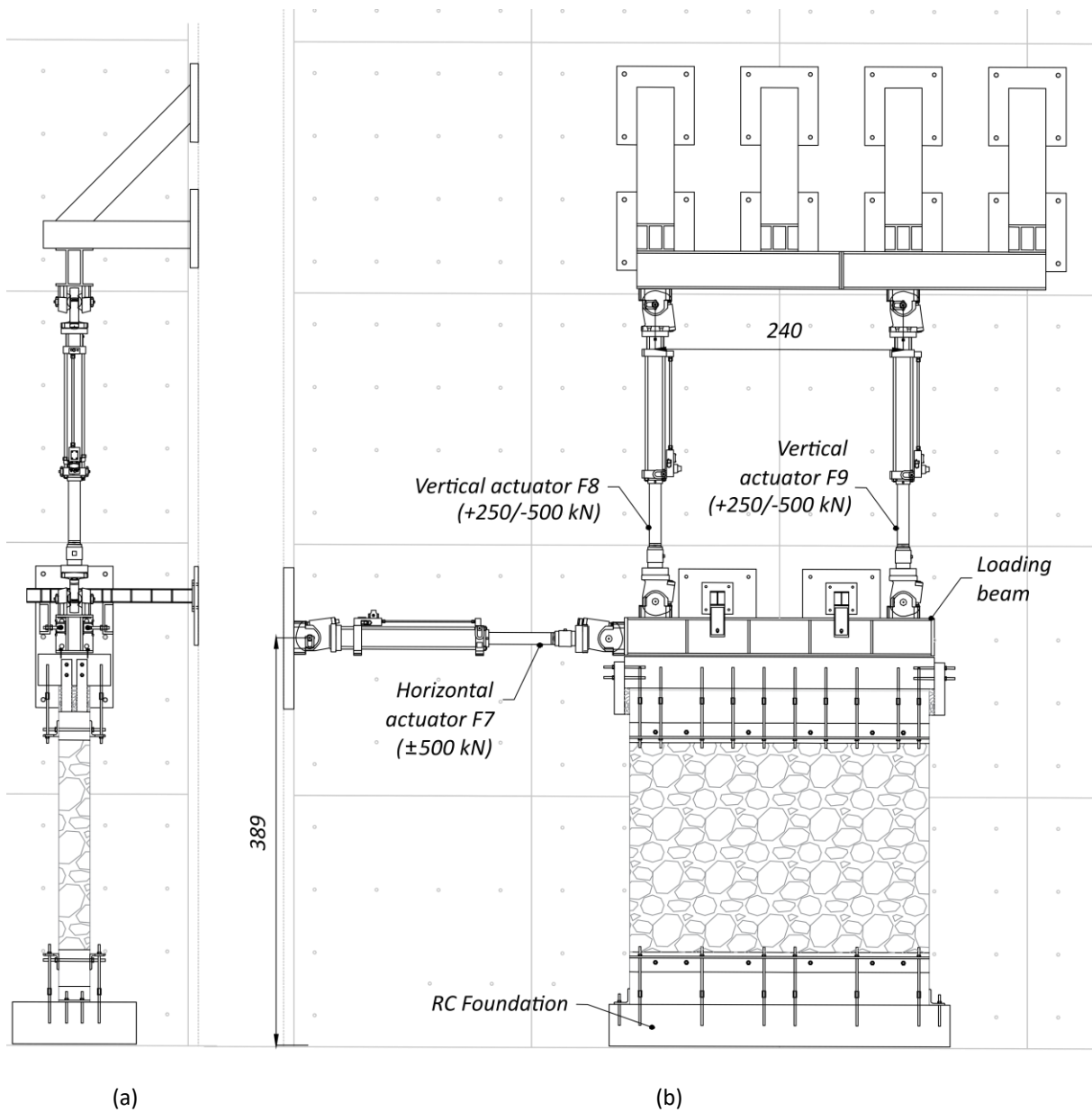


Figure 17. Quasi-static cyclic shear-compression test set-up for pier SQ_URM: (a) side view, and (b) front view. Units of cm.

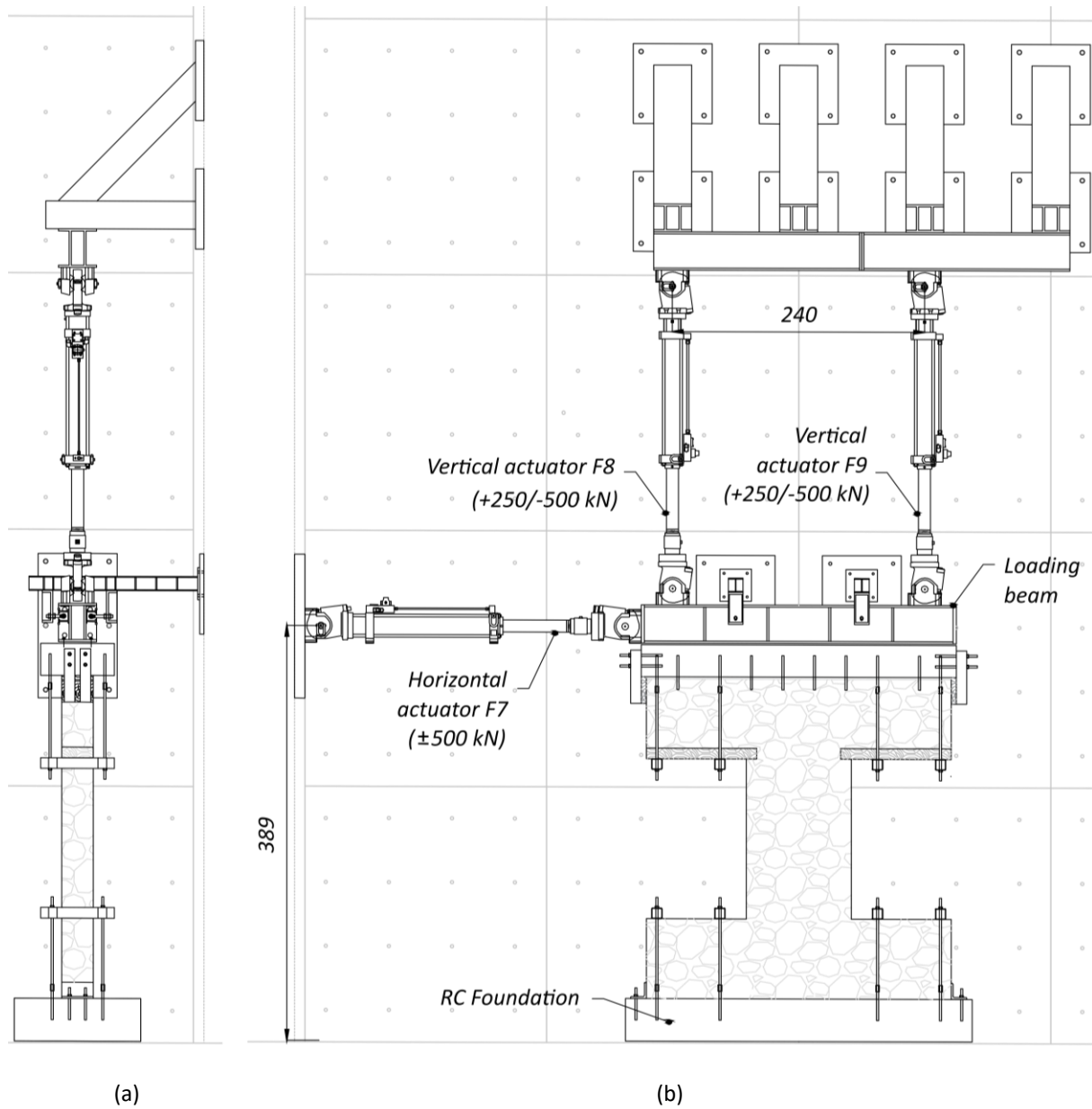


Figure 18. Quasi-static cyclic shear-compression test set-up for piers SL_URM, SL_CRM1, and SL_CRM2: (a) side view, and (b) front view. Units of cm.

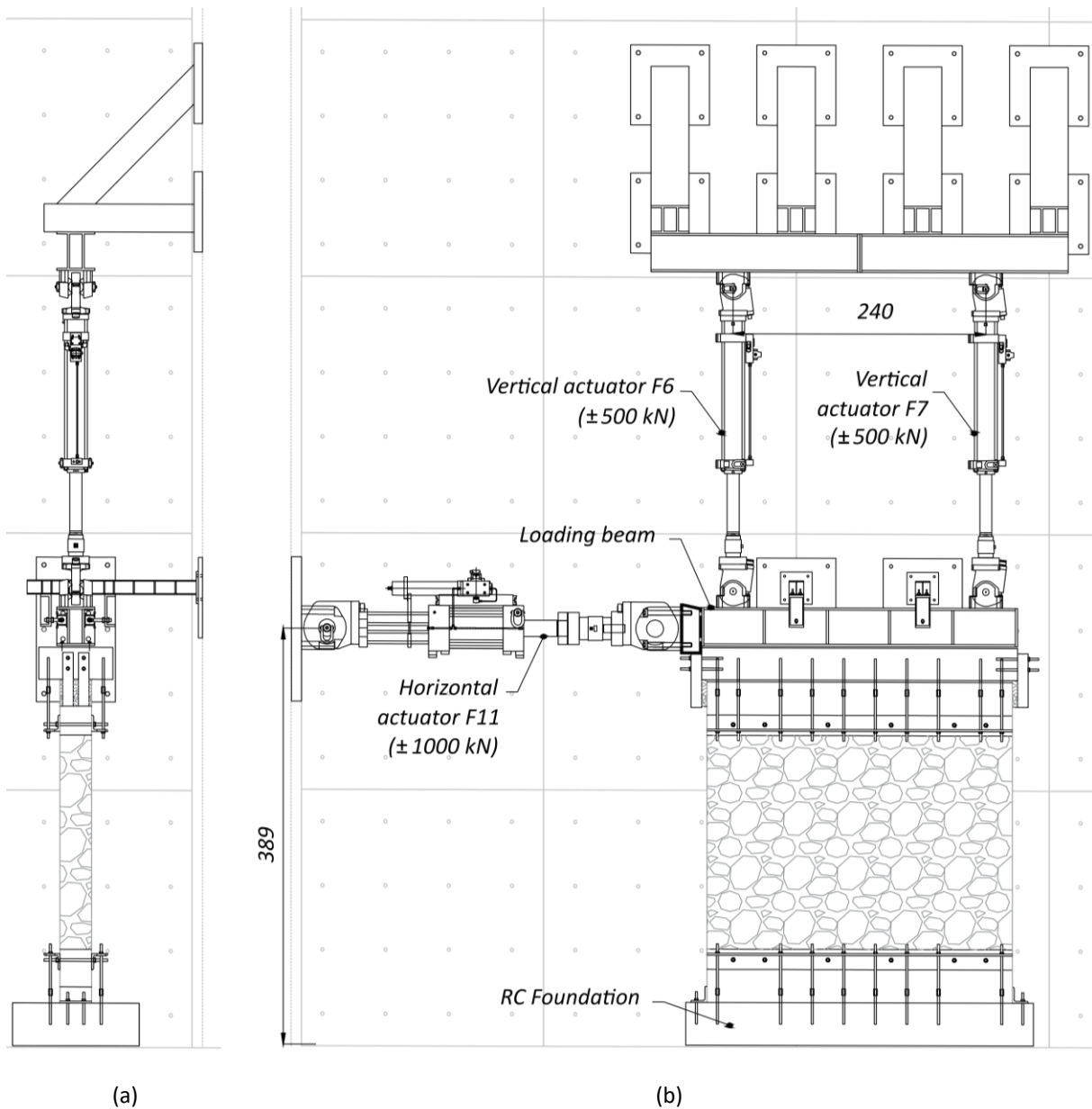


Figure 19. Quasi-static cyclic shear-compression test set-up for piers SQ_CRM1 and SQ_CRM2: (a) side view, and (b) front view. Units of cm.

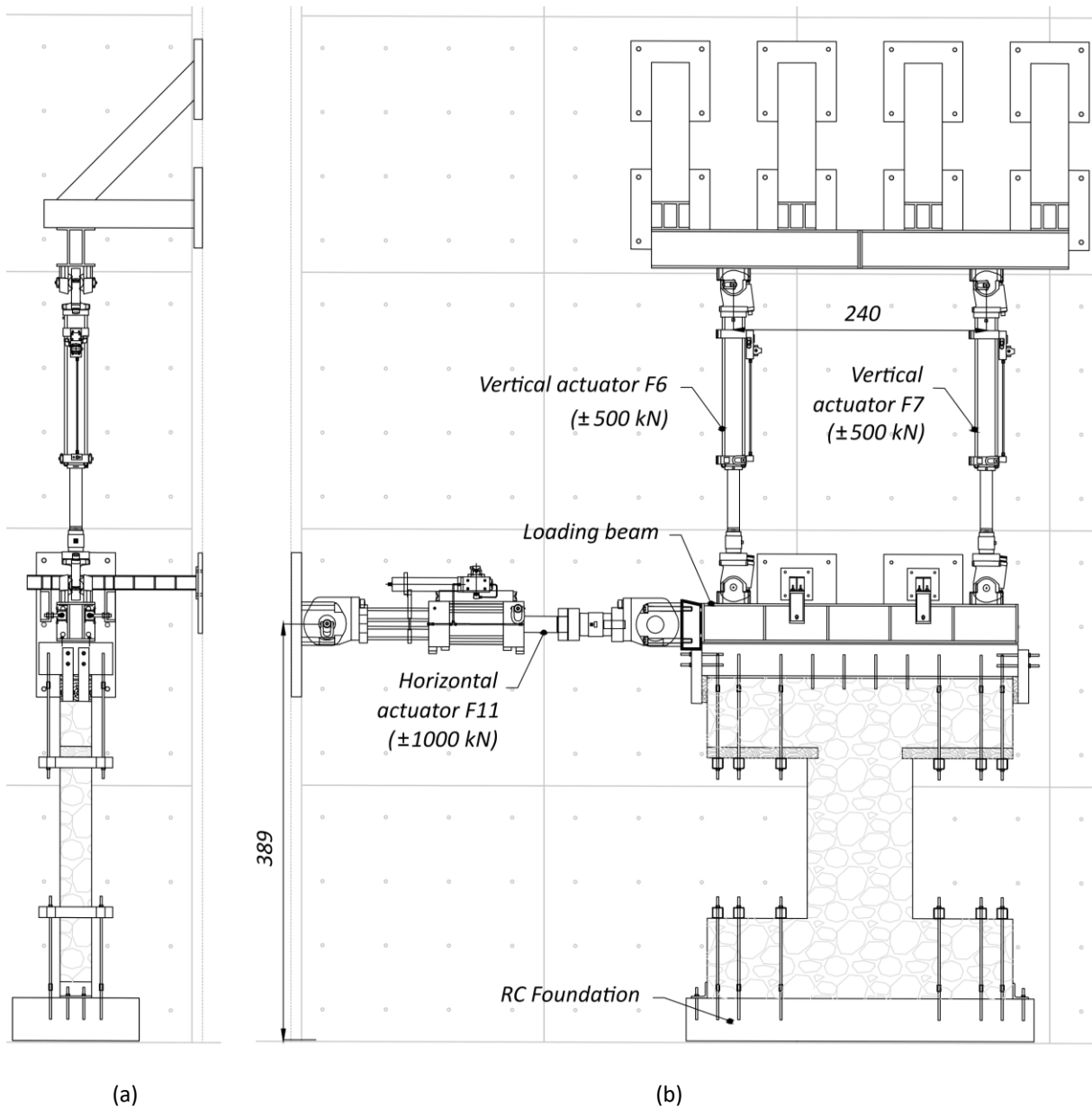


Figure 20. Quasi-static cyclic shear-compression test set-up for pier SL_FRM2: (a) side view, and (b) front view. Units of cm.

6.2 Testing protocol

All piers were tested under a constant axial force equal to 20% of the bare masonry compressive strength at their base, estimated from the vertical compression tests carried out in this experimental campaign, resulting in 119 and 344 kN for the slender and the squat piers, respectively. Subtracting the weights of the masonry pier (8.2 kN for the slender and 32 kN for the squat piers), top masonry or RC spandrel (11 kN), RC spreader beam (16 kN), steel loading beam (7.2 kN), and half horizontal actuator (3.6 kN for the 500-kN capacity actuator or 11 kN for the one with 1000-kN capacity), the constant sum of the forces applied by the pair of vertical actuators, P , was 66 kN for SL_FRM2, 73 kN for SL_URM, SL_CRM1, and SL_CRM2, 267 kN for SQ_CRM1 and SQ_CRM2, and 275 kN for SQ_URM.

To ensure a double-bending configuration, the vertical rotation of the pier top was restrained through a hybrid control of the vertical actuators. This control imposed the sum of the two forces to remain constant, while the two actuators to elongate or shorten by the same amount. The self-weight of the horizontal actuator, acting eccentrically on the pier, applied a bending moment at the specimen top; therefore, once the desired total vertical force, P , was achieved, it was necessary to impose a top rotation while keeping P constant, to compensate for this moment (Figure 21):

$$\begin{cases} F_L = \frac{P}{2} - \frac{W_H}{4} \cdot \left(1 + \frac{l_b}{d}\right) \\ F_R = \frac{P}{2} + \frac{W_H}{4} \cdot \left(1 + \frac{l_b}{d}\right) \end{cases} \quad (1)$$

In equation (1), F_L and F_R are the forces applied by the vertical left and right actuators, respectively; W_H is the weight of the horizontal actuator; d is the distance between the axes of the two vertical actuators, equal to 2.4 m; and l_b is the length of the beam, equal to 3 m.

The horizontal actuator was initially set in force control, and the specimens were subjected to a group of three push-and-pull cycles (F1) with a force amplitude of about 1/4 of the analytically predicted shear strength. The following group of three cycles (F2) had a force amplitude equal to 1.5 times the previous one. Then, a group of three displacement-controlled cycles (F3) was applied with amplitude multiple (about 2 to 3 times) of the displacement recorded during the F1 cycles; despite being displacement-controlled, these cycles depended on the outcomes of previous force-controlled cycles and are considered an F-group. Groups F2 and F3 were skipped in specimen SL_FRM2. From this point on, the protocol consisted of displacement-controlled groups of three cycles of increasing amplitude (D1 and following), targeting selected drift angles. The test was stopped when the specimen reached near-collapse conditions because of potentially dangerous damage patterns, a significant drop of lateral strength, or unstable behavior under constant vertical load.

Table 10 and Table 11 illustrate the horizontal cyclic sequences, specifying the cycle ID, the force or displacement rate, and the target horizontal force or top displacement, for the slender and squat specimens, respectively.

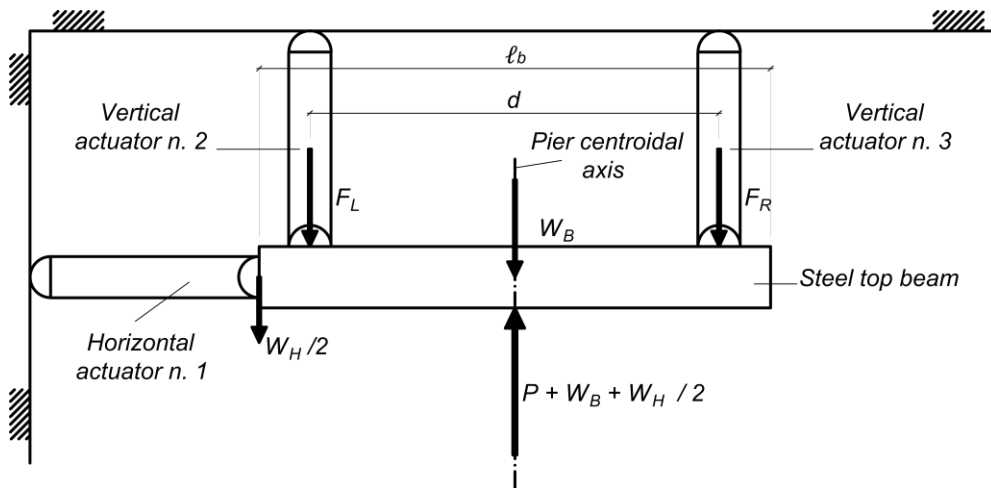


Figure 21. Scheme of the vertical forces applied to the RC beam.

Cycle ID	Control	SL_URM			SL_CRM1			SL_CRM2			SL_FRM2									
		Load velocity [kN/s]	Load velocity [mm/s]	Cycle target [kN]	Cycle target [mm]	Load velocity [kN/s]	Load velocity [mm/s]	Cycle target [kN]	Cycle target [mm]	Load velocity [kN/s]	Load velocity [mm/s]	Cycle target [kN]	Cycle target [mm]							
F1	Force	0.1	-	11	-	0.5	-	20	-	0.5	-	24	-	1.0	-	45	-			
F2	Force	0.25	-	17	-	0.5	-	25	-	0.5	-	30	-							
F3	Disp.	-	0.025	-	0.42	-	0.025	-	0.60	-	0.025	-	0.60	-	0.030	-	0.75			
D1	Disp.	-	0.030	-	0.75	-	0.030	-	0.75	-	0.030	-	0.75	-	0.036	-	1.13			
D2	Disp.	-	0.036	-	1.13	-	0.036	-	1.13	-	0.036	-	1.13	-	0.040	-	1.50			
D3	Disp.	-	0.040	-	1.50	-	0.040	-	1.50	-	0.040	-	1.50	-	0.045	-	2.25			
D4	Disp.	-	0.045	-	2.25	-	0.045	-	2.25	-	0.045	-	2.25	-	0.048	-	3.00			
D5	Disp.	-	0.048	-	3.00	-	0.048	-	3.00	-	0.048	-	3.00	-	0.060	-	3.75			
D6	Disp.	-	0.060	-	3.75	-	0.060	-	3.75	-	0.060	-	3.75	-	0.072	-	4.50			
D7	Disp.	-	0.072	-	4.50	-	0.072	-	4.50	-	0.072	-	4.50	-	0.096	-	6.00			
D8	Disp.	-	0.096	-	6.00	-	0.096	-	6.00	-	0.096	-	6.00	-	0.120	-	7.50			
D9	Disp.	-	0.120	-	7.50	-	0.120	-	7.50	-	0.120	-	7.50	-	0.144	-	9.00			
D10	Disp.	-	0.144	-	9.00	-	0.144	-	9.00	-	0.144	-	9.00	-	0.168	-	10.50			
D11	Disp.	-	0.168	-	10.50	-	0.168	-	10.50	-	0.168	-	10.50	-	0.192	-	12.00			
D12	Disp.	-	0.192	-	12.00	-	0.192	-	12.00	-	0.192	-	12.00	-	0.240	-	15.00			
D13	Disp.	-	0.240	-	15.00	-	0.240	-	15.00	-	0.240	-	15.00	-	0.300	-	18.75			
D14	Disp.	-	0.300	-	18.75	-	0.300	-	18.75	-	0.300	-	18.75	-	0.360	-	22.50			
D15	Disp.	-	0.360	-	22.50	-	0.360	-	22.50	-	0.360	-	22.50	-	0.420	-	26.25			
D16	Disp.																0.480	-	30.00	
D17	Disp.																-	0.720	-	45.00
D18	Disp.																-	0.960	-	60.00
D19	Disp.																-		-	

Table 11. Lateral loading protocol for the squat pier specimens, where three repetitions of each loading cycle were applied at every target drift ratio.

Cycle ID	Control	SQ_URM				SQ_CRM1				SQ_CRM2			
		Load velocity [kN/s]	Load velocity [mm/s]	Cycle target [kN]	Cycle target [mm]	Load velocity [kN/s]	Load velocity [mm/s]	Cycle target [kN]	Cycle target [mm]	Load velocity [kN/s]	Load velocity [mm/s]	Cycle target [kN]	Cycle target [mm]
F1	Force	0.5	-	45	-	1.5	-	75	-	2.0	-	104	-
F2	Force	0.5	-	67.5	-	1.5	-	113	-	2.0	-	156	-
F3	Disp.	-	0.025	-	0.5	-	0.025	-	0.6	-	0.025	-	0.75
D1	Disp.	-	0.040	-	1.0	-	0.040	-	1.0	-	0.040	-	1.0
D2	Disp.	-	0.048	-	1.5	-	0.048	-	1.5	-	0.048	-	1.5
D3	Disp.	-	0.053	-	2.0	-	0.053	-	2.0	-	0.053	-	2.0
D4	Disp.	-	0.060	-	3.00	-	0.060	-	3.00	-	0.060	-	3.00
D5	Disp.	-	0.064	-	4.00	-	0.064	-	4.00	-	0.064	-	4.00
D6	Disp.	-	0.080	-	5.00	-	0.080	-	5.00	-	0.080	-	5.00
D7	Disp.	-	0.096	-	6.00	-	0.096	-	6.00	-	0.096	-	6.00
D8	Disp.	-	0.128	-	8.00	-	0.128	-	8.00	-	0.128	-	8.00
D9	Disp.	-	0.160	-	10.00	-	0.160	-	10.00	-	0.160	-	10.00
D10	Disp.	-	-	-	-	-	0.192	-	12.00	-	0.192	-	12.00
D11	Disp.	-	-	-	-	-	-	-	-	-	0.224	-	14.00
D12	Disp.	-	-	-	-	-	-	-	-	-	0.256	-	16.00
D13	Disp.	-	-	-	-	-	-	-	-	-	0.320	-	20.00

6.3 Instrumentation

The specimens were densely instrumented with 40 displacement transducers (linear and wire potentiometers) to measure the in-plane deformation of the piers, their rigid body motions, eventual out-of-plane displacements, and possible relative movements between the specimens and the test set-up (Figure 22, Figure 23, and Figure 24). A high-accuracy displacement sensor (Temposonics) was installed on the loading beam aligned with the horizontal actuator, to control the applied lateral displacements. The accurate positions of the sensors can be found in the CAD file shared online with DOI 10.60756/euc-vbua48i530.

In addition, the east façade of the specimens (facing the laboratory) was left free of any instrument to apply a Digital Image Correlation (DIC) method and derive displacement and strain fields. For that, a white and black pattern was created on the specimen surface using brushes, as shown in Figure 25, and a high-resolution camera centered in front of the pier was used to take pictures every 10 seconds.



(a)

(b)

Figure 22. Instrumentation on the back and side façades: (a) squat, and (b) slender piers.

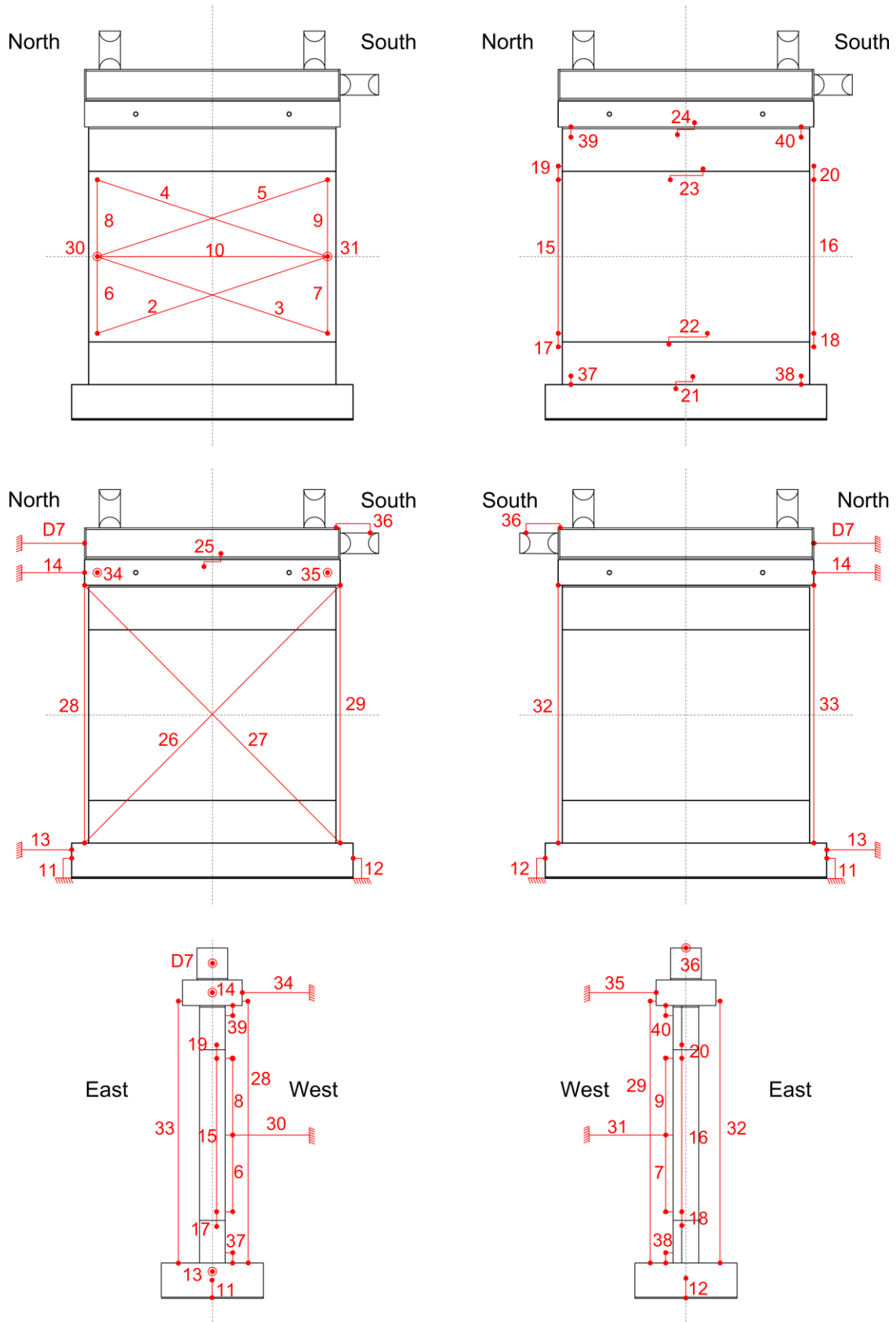


Figure 23. Instrumentation layout for the squat pier specimens.

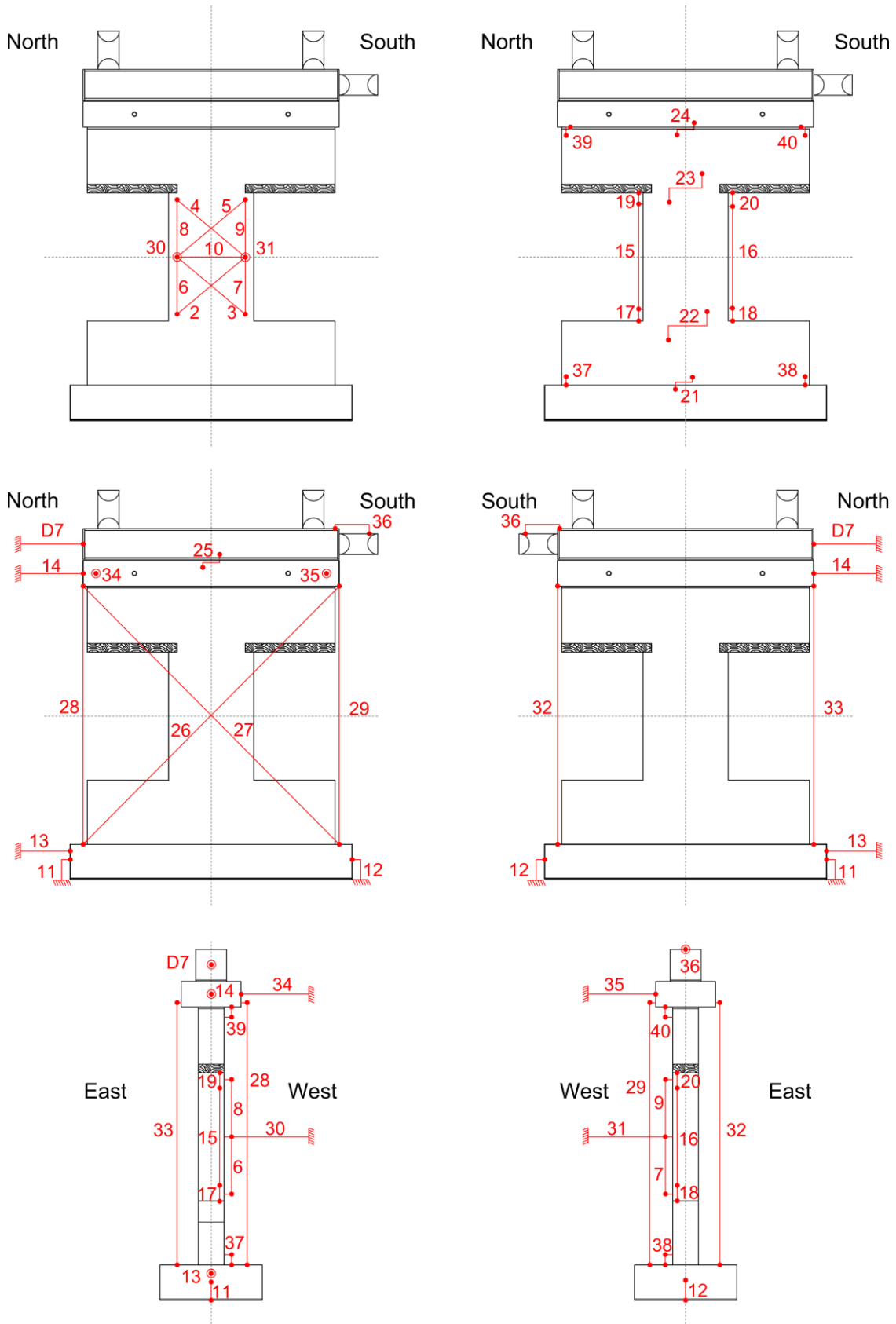


Figure 24. Instrumentation layout for the slender pier specimens.

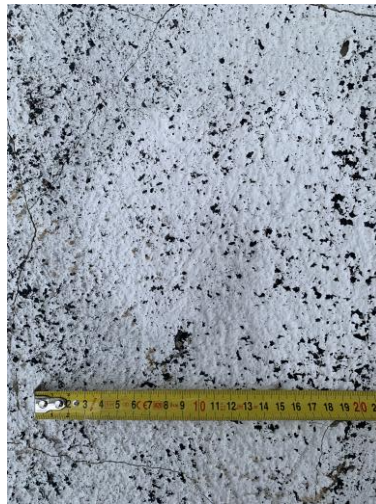


Figure 25. Random speckle pattern for the DIC method.

6.4 Data acquisition, processing, and distribution

All data sets are organized in .txt files shared online with DOI 10.60756/euc-vbua48i530 and named as “(Specimen designation)_(Cycle ID).txt”. Data are organized in columns corresponding to the time series recorded by each instrument, as presented in Table 12 and Table 13. In particular:

- i. Column 1 provides the time at a sampling rate of 8Hz;
- ii. Columns 2 through 40 provide the displacement time histories measured by linear and wire potentiometers;
- iii. Columns 41, 43, and 45 provide the forces applied by each of the two vertical and horizontal actuators, respectively;
- iv. Columns 42 and 44 provide the vertical displacements monitored by the actuators;
- v. Column 46 provides the horizontal displacement time history of the horizontal actuator measured by the Temposonics sensor.

Positive displacements correspond to elongation of the potentiometers. Positive forces are in tension; for the horizontal actuator, this corresponds to southward motions (pulling). All force and displacement recordings were filtered using a moving average window of 1 s. After filtering, the force and displacement histories were zeroed using the average of the first eight values, corresponding to the first second. The residual displacements accumulated at the end of the previous cycles were then added to the displacement-time series and are already included in the shared data. In some cases, due to the significant damage observed near the end of the test, certain sensors were removed in advance. From that point onward, the corresponding columns in the .txt file contain “NaN” entries.

It should be mentioned that the concrete cover started to detach and spall off from the top and bottom beams of the squat specimens before the end of the tests. This caused a fictitious displacement accumulation on transducers that measured rocking at those points (i.e. 17, 18, 19, e 20 from Figure 23). Therefore, the values from these potentiometers should be used carefully:

- Specimen SQ_URM from cycle 6;
- Specimen SQ_CRM1 from cycle 7;
- Specimen SQ_CRM2 from cycle 9.

ERIES-RESTORING Test Report

Table 12. Data matrix description for quasi-static cyclic shear-compression tests on slender piers.

Column No.	Sensor ID	Sensor type	Measured quantity / Instrument location	Units
1	-	-	Time	s
2	2	Linear pot.	Diagonal disp. along N-S direction, pier, lower part, W side	mm
3	3	Linear pot.	Diagonal disp along S-N direction, pier, lower part, W side	mm
4	4	Linear pot.	Diagonal disp along S-N direction, pier, top part, W side	mm
5	5	Linear pot.	Diagonal disp along N-S direction, pier, top part, W side	mm
6	6	Linear pot.	Vertical disp, pier, lower part, N-W corner	mm
7	7	Linear pot.	Vertical disp, pier, lower part, S-W corner	mm
8	8	Linear pot.	Vertical disp, pier, top part, N-W corner	mm
9	9	Linear pot.	Vertical disp, pier, top part, S-W corner	mm
10	10	Linear pot.	Horizontal disp., pier, mid-height, W side	mm
11	11	Linear pot.	Foundation vertical uplift, foundation - floor, N side	mm
12	12	Linear pot.	Foundation vertical uplift, foundation - floor, S side	mm
13	13	Linear pot.	Foundation horizontal slip, foundation - floor, N side	mm
14	14	Linear pot.	Horizontal disp., RC spreader beam, N side	mm
15	15	Linear pot.	Vertical disp., pier, intermediate, N side	mm
16	16	Linear pot.	Vertical disp., pier, intermediate, S side	mm
17	17	Linear pot.	Pier vertical uplift, pier – bottom spandrel, lower part, N side	mm
18	18	Linear pot.	Pier vertical uplift, pier – bottom spandrel, lower part, S side	mm
19	19	Linear pot.	Top spandrel vertical uplift, pier – top spandrel, top part, N side	mm
20	20	Linear pot.	Top spandrel vertical uplift, pier – top spandrel, top part, S side	mm
21	21	Linear pot.	Bottom spandrel horizontal slip, bottom spandrel – foundation, W side	mm
22	22	Linear pot.	Pier horizontal slip, pier – bottom spandrel, lower part, W side	mm
23	23	Linear pot.	Top spandrel horizontal slip, top spandrel – pier, W side	mm
24	24	Linear pot.	RC spreader beam horizontal slip, RC spreader beam – top spandrel, W side	mm
25	25	Linear pot.	RC spreader beam horizontal slip, RC spreader beam – load beam, W side	mm
26	26	Wire pot.	Diagonal disp. along N-S direction, foundation – RC spreader beam, W side	mm
27	27	Wire pot.	Diagonal disp. along S-N direction, foundation – RC spreader beam, W side	mm
28	28	Linear pot.	Vertical disp., foundation – RC spreader beam, N-W corner	mm
29	29	Linear pot.	Vertical disp., foundation – RC spreader beam, S-W corner	mm
30	30	Linear pot.	Out-of-plane, pier, mid-height, N-W corner	mm
31	31	Linear pot.	Out-of-plane, pier, mid-height, S-W corner	mm
32	32	Linear pot.	Vertical disp., foundation – RC spreader beam, S-E corner	mm
33	33	Linear pot.	Vertical disp., foundation – RC spreader beam, N-E corner	mm
34	34	Linear pot.	Out-of-plane, RC spreader beam, N-W corner	mm
35	35	Linear pot.	Out-of-plane, RC spreader beam, S-W corner	mm
36	36	Linear pot.	Actuator horizontal split, load beam – actuator, S side	mm
37	37	Linear pot.	Bottom spandrel vertical uplift, foundation – bottom spandrel, N-W corner	mm
38	38	Linear pot.	Bottom spandrel vertical uplift, foundation – bottom spandrel, S-W corner	mm
39	39	Linear pot.	Spreader beam vertical uplift, spandrel – RC spreader beam, N-W corner	mm
40	40	Linear pot.	Spreader beam vertical uplift, spandrel – RC spreader beam, S-W corner	mm
41	F8	Actuator load cell	Vertical actuator No. 8 vertical force, S side	kN
42	D8	Actuator elong.	Vertical actuator No. 8 vertical disp., S side	mm
43	F9	Actuator load cell	Vertical actuator No. 9 vertical force, N side	kN
44	D9	Actuator elong.	Vertical actuator No.9 vertical disp., N side	mm
45	F7	Actuator load cell	Horizontal actuator No. 7 vertical force, S side	kN
46	D7	Temposonics	Horizontal actuator No. 7 horizontal disp., S side	mm

ERIES-RESTORING Test Report

Table 13. Data matrix description for quasi-static cyclic shear-compression tests on squat piers.

Column No.	Sensor ID	Sensor type	Measured quantity / Instrument location	Units
1	-	-	Time	s
2	2	Wire potentiometer	Diagonal disp. along N-S direction, pier, lower part, W side	mm
3	3	Wire potentiometer	Diagonal disp along S-N direction, pier, lower part, W side	mm
4	4	Wire potentiometer	Diagonal disp along S-N direction, pier, top part, W side	mm
5	5	Wire potentiometer	Diagonal disp along N-S direction, pier, top part, W side	mm
6	6	Linear potentiometer	Vertical disp, pier, lower part, N-W corner	mm
7	7	Linear potentiometer	Vertical disp, pier, lower part, S-W corner	mm
8	8	Linear potentiometer	Vertical disp, pier, top part, N-W corner	mm
9	9	Linear potentiometer	Vertical disp, pier, top part, S-W corner	mm
10	10	Linear potentiometer	Horizontal disp., pier, mid-height, W side	mm
11	11	Linear potentiometer	Foundation vertical uplift, foundation - floor, N side	mm
12	12	Linear potentiometer	Foundation vertical uplift, foundation - floor, S side	mm
13	13	Linear potentiometer	Foundation horizontal slip, foundation - floor, N side	mm
14	14	Linear potentiometer	Horizontal disp., RC spreader beam, N side	mm
15	15	Linear potentiometer	Vertical disp., pier, intermediate, N side	mm
16	16	Linear potentiometer	Vertical disp., pier, intermediate, S side	mm
17	17	Linear potentiometer	Pier vertical uplift, pier – lower RC spandrel, lower part, N side	mm
18	18	Linear potentiometer	Pier vertical uplift, pier – lower RC spandrel, lower part, S side	mm
19	19	Linear potentiometer	Top RC band vertical uplift, pier – top RC spandrel, top part, N side	mm
20	20	Linear potentiometer	Top RC band vertical uplift, pier – top RC spandrel, top part, S side	mm
21	21	Linear potentiometer	Lower RC band horizontal slip, lower RC spandrel – foundation, W side	mm
22	22	Linear potentiometer	Pier horizontal slip, pier – lower RC spandrel, lower part, W side	mm
23	23	Linear potentiometer	Top RC band horizontal slip, top RC spandrel – pier, W side	mm
24	24	Linear potentiometer	RC spreader beam horiz. slip, RC spreader beam – top RC band, W side	mm
25	25	Linear potentiometer	RC spreader beam horiz. slip, RC spreader beam – load beam, W side	mm
26	26	Wire potentiometer	Diagonal disp. along N-S direction, foundation – RC spreader beam, W side	mm
27	27	Wire potentiometer	Diagonal disp. along S-N direction, foundation – RC spreader beam, W side	mm
28	28	Linear potentiometer	Vertical disp., foundation – RC spreader beam, N-W corner	mm
29	29	Linear potentiometer	Vertical disp., foundation – RC spreader beam, S-W corner	mm
30	30	Linear potentiometer	Out-of-plane, pier, mid-height, N-W corner	mm
31	31	Linear potentiometer	Out-of-plane, pier, mid-height, S-W corner	mm
32	32	Linear potentiometer	Vertical disp., foundation – RC spreader beam, S-E corner	mm
33	33	Linear potentiometer	Vertical disp., foundation – RC spreader beam, N-E corner	mm
34	34	Linear potentiometer	Out-of-plane, RC spreader beam, N-W corner	mm
35	35	Linear potentiometer	Out-of-plane, RC spreader beam, S-W corner	mm
36	36	Linear potentiometer	Actuator horizontal split, load beam – actuator, S side	mm
37	37	Linear potentiometer	Lower RC band vertical uplift, foundation – lower RC spandrel, N-W corner	mm
38	38	Linear potentiometer	Lower RC band vertical uplift, foundation – lower RC spandrel, S-W corner	mm
39	39	Linear potentiometer	Spreader beam vertical uplift, top RC band – RC spreader beam, N-W corner	mm
40	40	Linear potentiometer	Spreader beam vertical uplift, top RC band – RC spreader beam, S-W corner	mm
41	F8	Actuator load cell	Vertical actuator No. 8 vertical force, S side	kN
42	D8	Actuator elongation	Vertical actuator No. 8 vertical disp., S side	mm
43	F9	Actuator load cell	Vertical actuator No. 9 vertical force, N side	kN
44	D9	Actuator elongation	Vertical actuator No.9 vertical disp., N side	mm
45	F7	Actuator load cell	Horizontal actuator No. 7 vertical force, S side	kN
46	D7	Temposonics	Horizontal actuator No. 7 horizontal disp., S side	mm

For each specimen, a dedicated DIC sub-folder is provided containing the DIC photographs captured during the tests. Given the large volume of data generated during the experimental campaign, only selected images, corresponding to key displacement points such as zero, minimum, and maximum displacements within each cycle, have been included. Each sub-folder also contains a text file specifying the exact timestamps at which these images were taken, named “(Specimen designation)_name_changes_and_timestamps.txt”.

Additionally, the sub-folder includes information on the absolute time at which each loading cycle began in the file “(Specimen designation)_Absolute Starting Time for DIC.txt”. The instrumentation data files, named “(Specimen designation)_(Cycle ID).txt”, contain time series sampled at a frequency of 8 Hz, and provide a relative time column reset to zero at the beginning of each cycle.

Although the data acquisition is based on relative timing, the inclusion of the absolute start time of each cycle allows for the reconstruction of absolute time for any data point, by summing the relative time (from the instrumentation data file) with the corresponding cycle's starting time. This enables a precise correlation between the conventional instrumentation data and the DIC images. As a result, both datasets can be synchronized to enable detailed analysis of the structural response using both electrical and visual information.

Acknowledgments

The work presented in the present report is part of the transnational access project “ERIES – RESTORING”, supported by the Engineering Research Infrastructures for European Synergies (ERIES) project (www.eries.eu), which has received funding from the European Union’s Horizon Europe Framework Programme under Grant Agreement No. 101058684.

The authors would like to acknowledge the help provided by the staff of the EUCENTRE Foundation and of DICAr/UniPV, the material support by Laterlite S.p.A., the financial support by the European Union – NextGeneration EU through the postdoctoral grant Margarita Salas, the financial support by the Foundation for Science and Technology (FCT) through a PhD scholarship [grant number SFRH/BD/145571/2019] and CERIS project UIDB/04625/2025, and the financial support by DPC-ReLUIS project (2024-2026) through WP5 “Integrated and sustainable interventions for existing buildings” and WP10 “Masonry constructions” funded by the Italian Department of Civil Protection.

Note that the opinions and conclusions presented by the authors do not necessarily reflect those of the funding entities.

References

- ASTM International (2015). *E519-15. Standard Test Method for Diagonal Tension (Shear) in Masonry Assemblages*, ASTM International, West Conshohocken, PA, USA.
- CEN (1998). *EN 1052-1:1998. Methods of test for masonry - Part 1: Determination of compressive strength*, European Committee for Standardization, Brussels, Belgium.
- CEN (2006). *EN 1015-11:1999/A1:2006. Methods of test for mortar for masonry - Part 11: Determination of flexural and compressive strength of hardened mortar*, European Committee for Standardization, Brussels, Belgium.
- Guerrini, G., Bruggi, A., Urso, S., Quaini, M., & Penna, A. (2021). Diagonal Compression Tests on Stone Masonry Wallettes Jacketed with Different Techniques. *Proceedings of Murico7 – Mechanics of masonry structures strengthened with composite materials*.
- Magenes, G., Penna, A., Galasco, A., Rota, M. (2010). Experimental characterization of stone masonry mechanical properties. *Proceedings of the 8th International Masonry Conference*, July 4-7, Dresden, Germany, 247-256.
- RILEM (1991). *LUM B6. Diagonal Tensile Strength Tests of Small Wall Specimens*, International Union of Laboratories and Experts in Construction Materials, Systems and Structures, E. & F.N. Spon Ltd., London, UK. DOI: 10.1617/2351580117.152
- Senaldi, I., Guerrini, G., Scherini, S., Morganti, S., Magenes, G., Beyer, K., Penna, A. (2018). Natural stone masonry characterization for the shaking-table test of a scaled building specimen. *Proceedings of the 10th International Masonry Conference*, Milan, Italy.